

Femtosecond dynamics of photoinduced molecular detachment from halogenated alkanes. I. Transition state dynamics and product channel coherence

Una Marvet, Qingguo Zhang,^{a)} Emily J. Brown, and Marcos Dantus^{b)}

Department of Chemistry and Center for Fundamental Materials Research, Michigan State University, East Lansing, Michigan 48824-1322

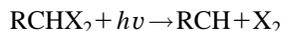
(Received 30 January 1998; accepted 12 June 1998)

The direct observation of the photoinduced molecular detachment of halogens X_2 from halogenated alkanes $RCHX_2$ is presented. Three-photon excitation at 312 nm produces molecular halogens and a carbene; the halogen products are formed predominantly in the D' state. Femtosecond pump-probe spectroscopy of the reaction reveals a fast ($\tau < 50$ fs) dissociation with no evidence of intramolecular vibrational redistribution. This is consistent with a prompt dissociation without intermediates. The experimental results demonstrate vibrational coherence in the halogen product, which requires that the reaction proceed by a concerted mechanism. © 1998 American Institute of Physics. [S0021-9606(98)02335-6]

I. INTRODUCTION

Under high energy excitation, several simple polyatomic molecules have been known to dissociate to yield molecular photofragments, e.g., $H_2O \rightarrow H_2 + O$, $NH_3 \rightarrow NH + H_2$, $H_2CO \rightarrow H_2 + CO$ (Ref. 1) and $COCl_2 \rightarrow Cl_2 + CO$ (Ref. 2). Instead of breaking a single bond as in the majority of photodissociation processes studied to date, this photoinduced molecular detachment or molecular photodetachment process involves breakage and formation of more than one bond. Several dihaloalkanes, most notably CH_2IBr (Ref. 3) and CH_2I_2 (Refs. 4–8), have also been known to undergo molecular detachment processes. As this study demonstrates, many other gem-dihaloalkanes, e.g., CH_2Br_2 , CH_2Cl_2 and $n-C_4H_8I_2$, also photodissociate to yield dihalogen molecules as photofragments.

This paper is the first of a series in which the time-resolved dynamics of photoinduced molecular detachment processes will be examined. The reaction of interest to this study is the molecular detachment of X_2 from $RCHX_2$,



(where $X = Cl, Br$ or I). Possible mechanisms for this reaction are shown schematically in Fig. 1. In (a) the two carbon-halogen bonds break sequentially and X_2 forms later by a collisional process. This is a stepwise mechanism; the molecular halogen is a secondary product. The pathway shown in Fig. 1(b) is concerted, i.e., it proceeds in a single kinetic step. Breaking of the two carbon-halogen bonds is initiated at the same time and proceeds at the same rate. An interhalogen bond forms before the carbon-halogen bonds are completely broken. In the asynchronous concerted mechanism (c) the reaction also proceeds in a single kinetic step. In this case, however, the rate at which the two carbon-

halogen bonds break is different. Again, the interhalogen bond forms before the halogens are completely dissociated from the carbene. In this paper, the femtosecond transition state dynamics and vibrational coherence in the halogen product will be studied in detail. In the companion article (referred to as paper II henceforth), the rotational anisotropy of the halogen product will be used to identify the mechanism of one dissociation pathway leading to the formation of I_2 .⁹

The spectroscopy and photodissociation dynamics of CH_2I_2 have received a great deal of attention over the past two decades.^{6,7,10–24} Most of these studies are concerned with the photodissociation dynamics of low-lying excited electronic states,^{10–21} which dissociate to produce CH_2I and I fragments with I in either its ground $^2P_{3/2}$ state or its spin-orbit excited $^2P_{1/2}$ state. However, upon high energy excitation, CH_2I_2 has been known to undergo molecular detachment to yield I_2 in highly excited electronic states, i.e., $CH_2I_2 \rightarrow CH_2 + I_2$. Following the first observation of this pathway by Style and co-workers,^{4,5} Black⁸ and Okabe *et al.*⁷ conducted thorough spectroscopic investigations of the photodissociation process. Black showed that the I_2 342 nm fluorescence intensity reaches its maximum value within 10 ns of excitation, which is considerably less than 50 μs , the mean collision time under their experimental conditions.⁸ This suggests that I_2 formation is a primary event. Although the quantum yield measurements for I_2 342 nm fluorescence determined by Black ($\phi_f = 0.002$, excitation at 121.6 nm)⁸ differ from those of Okabe *et al.* ($\phi_f = 0.006$, excitation at 123.6 nm),⁷ they both indicate that the molecular detachment process represents only a minor relaxation pathway for the photoexcitation. From analysis of the dispersed fluorescence spectra, Okabe *et al.* also found moderately high vibrational excitation (v' up to 35) in the nascent I_2 fragment.

The short time dynamics of CH_2I_2 has been studied recently by many groups using both femtosecond time-resolved techniques^{19,20} and resonance Raman spectroscopic

^{a)}Current address: George R. Harrison Spectroscopy Laboratory, Massachusetts Institute of Technology, Cambridge, MA 02139.

^{b)}Author to whom correspondence should be addressed.

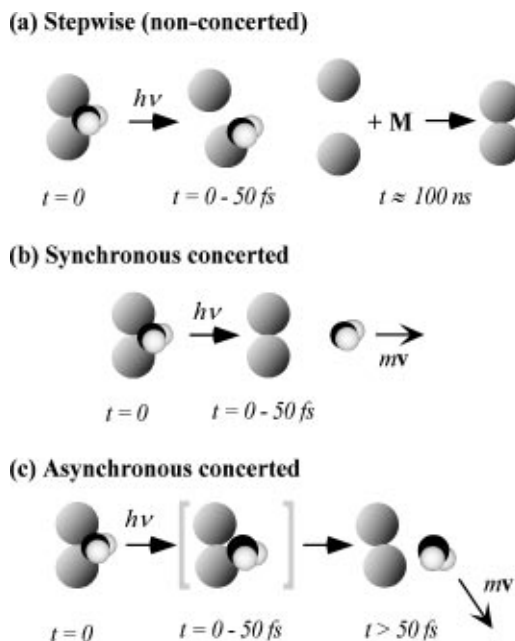


FIG. 1. Schematic of possible mechanisms for the photoinduced molecular detachment of X_2 from gem-dihaloalkanes. The time scales given for these mechanisms are based on our time-resolved measurements. Three processes are depicted: (a) Stepwise (nonconcerted) mechanism; one halogen-carbon bond breaks some time before the other. Halogen products are formed later, by collisional association. M represents a third body in the collision process, which is required for formation of a diatomic. No coherence is expected from this pathway. (b) In the synchronous concerted mechanism, breaking of the two carbon-halogen bonds is initiated at the same time and proceeds at the same rate. An interhalogen bond forms before the carbon-halogen bonds are completely broken. This pathway has a symmetric transition state and preserves the C_{2v} symmetry of the parent. This mechanism would be expected to produce molecular halogen products with a small rotational angular momentum and a significant degree of vibrational excitation. (c) In the asynchronous concerted mechanism the reaction proceeds in a single kinetic step, as described above. In this case, however, the rate at which the two carbon-halogen bonds break is different. Again, the interhalogen bond forms before the halogens are completely dissociated from the carbene. This mechanism produces halogen molecules with a large rotational angular momentum.

measurements.¹⁵⁻¹⁸ However, all these studies are concerned with the photodissociation dynamics for breaking of a single C-I bond. It was found that the dissociation process takes place in less than 120 fs^{19,20} and that the I-C-I symmetric stretching mode is initially activated, which leads to breaking of one of the two C-I bonds by coupling to the I-C-I anti-symmetric stretching mode.¹⁵⁻¹⁸

A series of efforts has been made in our group to investigate the molecular photodetachment dynamics of CH_2I_2 and its derivatives.^{9,25-28} The existence of coherent vibrational motion in the I_2 photofragment has been observed. This is an indication that the molecular photodetachment process is concerted, i.e., the breaking of the two C-I bonds and the formation of the I-I bond occur in a single kinetic step.

This study and paper II⁹ represent a continuation of our effort to elucidate detailed photodissociation dynamics of gem-dihaloalkanes using femtosecond pump-probe techniques. The experimental setup will be described in Sec. II of this paper. Dispersed fluorescence spectra and time-resolved transients following multiphoton excitation of CH_2I_2 ,

CH_2Br_2 and CH_2Cl_2 will be presented in Sec. III. In Sec. IV, detailed analysis of the fluorescence spectra, the transition state dynamics and the photofragment dynamics will be presented. The experimental data form the basis for a discussion of the molecular detachment mechanism of this reaction.

II. EXPERIMENT

The laser system used for these experiments is a home built colliding pulse mode-locked dye laser (CPM), pumped by an Ar^+ laser. The output from the CPM is centered at 624 nm and is amplified using a four-stage dye amplifier pumped by a 30 Hz Nd-YAG laser. A double-pass prism pair recompresses the pulses after amplification to produce 50 fs pulses with an average energy of 0.5 mJ per pulse. The pulses were characterized using a frequency-resolved optical gating (FROG) method.

Pump and probe pulses were prepared using a Mach-Zehnder interferometer. A 0.1 mm KDP second harmonic generation (SHG) crystal in the fixed arm was used to produce the 312 nm pump pulses. The two beams were collinearly recombined using a dichroic beam splitter and focused into the sample cell. Laser induced fluorescence (LIF) was detected perpendicular to the laser path using a 0.27 m monochromator and a photomultiplier tube (PMT). The signal was collected by a boxcar integrator and stored in a computer for analysis. Spectra were wavelength calibrated using mercury lamp emission.

All experiments were performed on neat vapor ($\sim 0.1-10$ Torr) of the relevant alkyl halide in a static quartz cell (ice baths were used when necessary). The purity of the samples was checked by nuclear magnetic resonance (NMR) and gas chromatography (GC). Dehydrated sodium thiosulfate was used as a scavenger to prevent the accumulation of molecular halogens. The 312 nm (pump) pulse initiates the reaction by multiphoton excitation of the sample vapor; dissociation products are detected by fluorescence. To obtain time-resolved data, the probe pulse at 624 nm was used to deplete the population of halogen molecules in the fluorescent state. Sweeping the time delay between the pump and probe pulses thus yields a transient that reflects the temporal evolution of the reaction. At each pump-probe time delay, the signal is collected for 10 laser shots; pulses with energy more than one standard deviation from the mean are discarded. Typical transients contain data from 200 different time delays and are averages of 100 scans.

III. RESULTS

The dispersed fluorescence spectra resulting from multiphoton excitation of CH_2I_2 , CH_2Br_2 and CH_2Cl_2 at 312 nm are presented in Fig. 2. The fluorescence intensity has not been corrected for detection efficiency of the spectrometer. Most of the spectral features can be assigned to fluorescence from nascent halogen molecules resulting from photodissociation of the parent. One of the most striking observations is that in all cases the principal fluorescent product is a halogen molecule in the D' state, which is an ion-pair state, i.e., it correlates to $X^+ + X^-$.²⁹⁻³⁴ In the case of CH_2I_2 , this is consistent with frequency-resolved studies of photodissociation

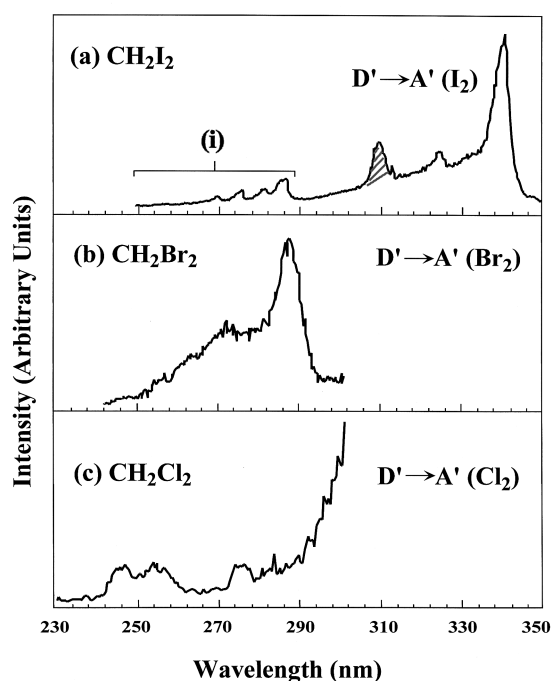


FIG. 2. Fluorescence spectra resulting from the multiphoton dissociation of gem-dihaloalkanes. All spectra were obtained by gas-phase excitation at 312 nm in a static cell. (a) From CH_2I_2 . The dominant fluorescence is between 300 and 350 nm and can be assigned to the $\text{I}_2 D' \rightarrow A'$ transition. A small amount of laser scatter is detected at 312 nm (shaded). The region marked (i) indicates fluorescence produced by other ion-pair states of I_2 ; this region will be investigated in detail in paper (II). (b) From CH_2Br_2 , showing the $D' \rightarrow A'$ fluorescence of Br_2 . (c) From CH_2Cl_2 ; again, a characteristic $D' \rightarrow A'$ fluorescence is observed, this time due to Cl_2 . In this case the signal is weak. The increased signal from 280 toward 310 nm is due to laser scatter.

at high energies.⁴⁻⁷ The $\text{I}_2 D' \rightarrow A'$ fluorescence is well characterized and is commonly observed when I_2 is excited in the presence of buffer gases.²⁹⁻³¹ Under these circumstances the D' state is populated by collisional relaxation from other ion-pair states; this process is very efficient. However, the pressure in the reaction cell is ~ 1 Torr, which precludes the possibility of forming $\text{I}_2(D')$ by collisional relaxation, since the time between collisions at this pressure, ≈ 130 ns, is much longer than the fluorescence lifetime of other ion-pair states (~ 10 ns).³⁵ In addition, a collisional formation process would produce a rise time on the order of 100 ns. The observed signal had a very rapid rise time and was collected with a boxcar integrator having a 50 ns gate. The D' state of halogens is optically inaccessible from the ground state; observation of this transition therefore indicates that the I_2 fluorescence is originating from a nascent dissociation product.

It can be seen from the CH_2I_2 spectrum that there are also fluorescence bands between 250 and 290 nm; the $f(3^3\Pi_{0g}^+) \rightarrow A(3^3\Pi_{1u})$ (Ref. 36), $F(1^1\Sigma_{0u}^+) \rightarrow X(1^1\Sigma_{0g}^+)$ (Ref. 36), $f'(1^1\Sigma_{0g}^+) \rightarrow B(3^3\Pi_{0u}^+)$ (Ref. 37), $g(0_g^-) \rightarrow 3^3\Pi(0_u^-)$ (Ref. 36) and $G(1g) \rightarrow A(3^3\Pi_{1u})$ (Ref. 36) transitions of I_2 fluoresce in this region. The integrated intensity of the fluorescence in the 250–290 nm region relative to the 290–350 nm region is approximately 10%. A detailed analysis of the signal observed in this region is presented in paper II.⁹

If the $f(3^3\Pi_{0g}^+)$ state of I_2 were populated, we would also

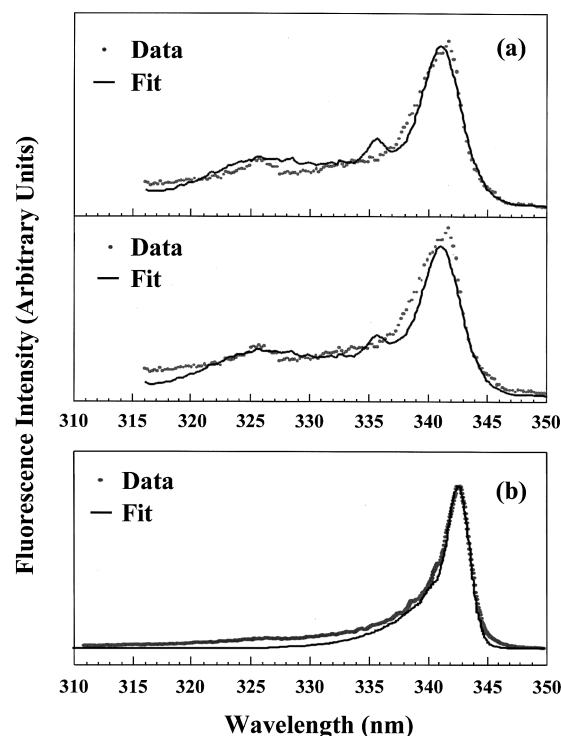


FIG. 3. Dispersed fluorescence spectra from the D' state of I_2 . (a) Fit to the $\text{I}_2 D' \rightarrow A'$ spectrum produced from the dissociation of CH_2I_2 . The top panel shows the fit using only $D' \rightarrow A'$ fluorescence; in the lower panel, fluorescence due to the $f \rightarrow B$ transition was also taken into account (see text). (b) Fit to a collisionally relaxed (Boltzmann) distribution of vibrational levels of the D' state. The data were obtained from a cell containing I_2 vapor and Ar gas at 100 Torr.

expect to see fluorescence in the 300–350 nm region of the spectrum, assignable to the $f \rightarrow B$ transition. Figure 3(a) shows the fit to the spectrum of the I_2 fluorescence produced in this region by photodissociation of CH_2I_2 . The fit shown in the top panel in Fig. 3(a) was obtained by assuming that all the fluorescence in this region was produced by the $\text{I}_2 (D' \rightarrow A')$ transition; the second panel shows the same data fit with $\approx 30\%$ (optimized for fit) of $f \rightarrow B$ fluorescence. Although there are still deviations from the fit, the second panel shows a better correspondence to the data than in the first panel, particularly in the region between 322 and 337 nm. Remaining differences may be due to errors in the assumed vibrational distribution in the f state; we will investigate this further. The fits were both obtained by using a least-squares routine and by assuming a Gaussian distribution of vibrational levels in the D' state; the observed fits correspond to a central vibrational level $v_{\text{max}}=9$.

The $D' \rightarrow A'$ fluorescence that would be observed from collisionally relaxed $\text{I}_2(D')$ molecules was also simulated; Fig. 3(b) shows a comparison of the simulation with the dispersed fluorescence obtained from a sample of I_2 in 100 Torr of Ar at ambient temperature. This is expected to produce a Boltzmann population of vibrational states in the D' electronic state of I_2 . Figure 3(b) shows that the match between the simulated spectrum and the experimental data is quite good. It is clear from Figs. 3(a) and 3(b) that the $\text{I}_2(D')$

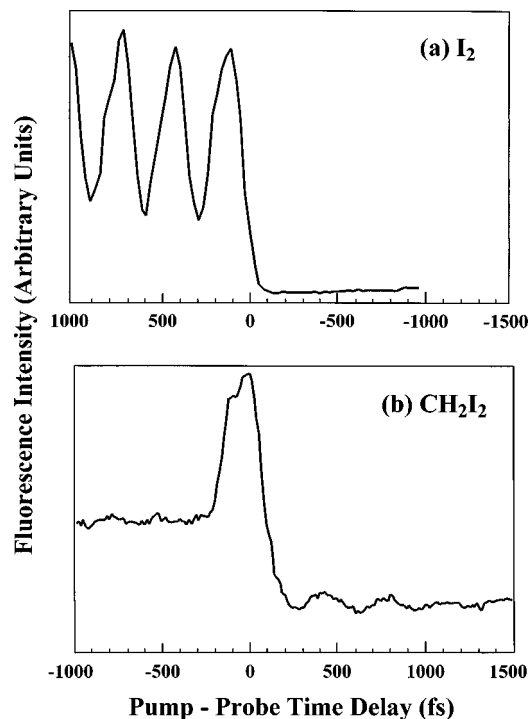


FIG. 4. Time-resolved data of I_2 (refer also to Fig. 5). (a) From iodine vapor (neat), showing no signal at negative times and vibrational coherence characteristic of $I_2(B)$ at positive times. A 624 nm (pump) pulse excites I_2 to the B state; subsequent absorption of a 312 nm pulse causes transition to the E and f states; signal is $f \rightarrow B$ fluorescence at 340 nm. (b) From the dissociation of CH_2I_2 . Multiphoton absorption of 312 nm photons causes photoinduced molecular detachment of I_2 in the D' state. At positive times, fluorescence at 340 nm from the $D' \rightarrow A'$ transition is depleted by the 624 nm (probe) pulse. Observation of vibrational modulation in the depletion signal indicates that a coherent wave packet is generated in the D' state of I_2 , see Fig. 5(b). Note that for the I_2 transient, positive time corresponds to the 624 nm pulse arriving at the cell first; for the CH_2I_2 sample, positive time is when the 312 nm pulse arrives first.

population resulting from the photodissociation of CH_2I_2 can not be represented by a Boltzmann distribution.

To further confirm that the observed fluorescence signal does not originate from background I_2 in the cell, time-resolved data of the fluorescence signal at 340 nm were collected for two cells, each containing CH_2I_2 or I_2 . Figure 4(a) shows the results from the I_2 cell. When I_2 absorbs a photon of energy 2 eV (provided by the 624 nm pulse), it is excited to the B state as shown in Fig. 5(a). Absorption of an additional 4 eV from the 312 nm pulse causes excitation to the ion-pair states E and f , which are fluorescent. The transient obtained by detecting the 340 nm fluorescence from the $f \rightarrow B$ transition is shown in Fig. 4(a). Because ground-state I_2 does not absorb at 4 eV, no fluorescence signal is observed from the iodine cell when the 312 nm pulse arrives first (negative time). As the pulses become overlapped in time (time zero), the ion-pair states are populated and the fluorescent signal begins to appear. At positive times (624 nm pulse arriving first), modulation in the fluorescence intensity can be seen as the pump-probe time delay is scanned. This is a Franck-Condon effect caused by oscillation of the wave packet prepared by the 624 nm pulse on the potential energy surface of the B state. This phenomenon has been exten-

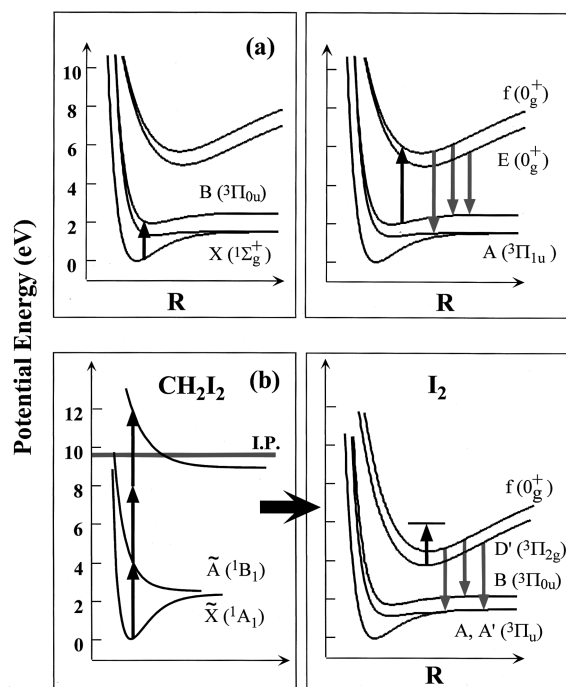


FIG. 5. Excitation schemes for I_2 and CH_2I_2 showing how observed time-dependent fluorescence is generated. (I.P. refers to the ionization potential of the molecule.) (a) From I_2 vapor (neat). The 624 nm (pump) pulse excites I_2 to the B state. Subsequently, a 312 nm pulse promotes the excited I_2 molecules to the E and f states; fluorescence from the $f \rightarrow B$ transition is detected at 340 nm. The vibrational oscillations observed in Fig. 4(a) are produced by Franck-Condon transitions from the wave packet oscillating on the B state potential energy surface. (b) From CH_2I_2 vapor. Initially, the molecule undergoes multiphoton absorption of the 312 nm (pump) pulse. This causes it to dissociate, producing I_2 in the D' state. Absorption of a 624 nm (probe) pulse by the iodine depletes the population of the D' state. Depletion efficiency tracks the progress of the reaction and is monitored by detecting the $D' \rightarrow A'$ fluorescence at 340 nm. Note that the probe transition may not be as represented; there are a number of optically accessible dissociative I_2 states 2 eV below the D' state.

sively studied and produces vibrational oscillations characteristic of the B state of I_2 .³⁸

By contrast, examine the transient produced from the CH_2I_2 cell, shown in Fig. 4(b). The pump pulse at 312 nm causes the parent molecule to dissociate, producing I_2 in the D' state, which is fluorescent. At positive times (312 nm pulse arriving first), the 624 nm (probe) pulse depletes the population of the D' state, causing a drop in signal intensity, see Figs. 4(b) and 5(b). Unlike the case of the iodine sample, however, the signal does not become zero when the 312 nm pulse arrives first; it is simply at a lower level. At negative times, the probe pulse is unable to deplete the D' state, so the signal is at a higher level than at positive times. Several other differences are also apparent; the signal from the CH_2I_2 sample shows no modulation for negative time delays, but periodic modulations in the depleted fluorescence can be seen at positive time. It is clear from the comparisons above that the I_2 fluorescence signal being produced from the CH_2I_2 sample is a result of photoinduced molecular detachment of I_2 molecules and not background iodine in the cell.

Since the threshold for production of I_2 from the photodissociation of CH_2I_2 is 9.4 eV^{7,8} and the energy of a 312 nm photon is 4 eV, multiphoton absorption is required to pro-

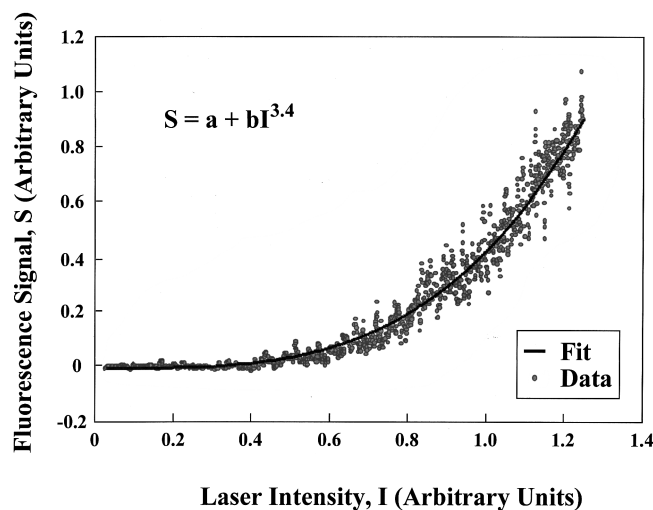


FIG. 6. Power dependence data for the photodetachment of $I_2(D')$ from CH_2I_2 . Data are plotted as fluorescence intensity at 340 versus intensity of the 312 nm laser pulse. The least-squares fit displayed was obtained with a dependence of the fluorescence intensity on 312 nm laser power of 3.4.

duce the observed fluorescence signal. Reliable power dependence measurements for high order nonlinear processes of this type are inherently difficult because of the necessity for a wide dynamic detection range and because these types of processes can easily become saturated. We have taken care in measuring the power dependence to ensure that the laser pulse does not saturate either the molecular transition or the instrumental response even when it is at its most intense. Power dependence data were collected by deliberately defeating the synchronization between the oscillator and amplifier of the femtosecond laser; this produces a train of pulses with a wide range of random intensities. Several hundred points were then recorded by simultaneously detecting the fluorescence signal from the product cell using the PMT and the laser intensity using a fast photodiode, taking care not to saturate either detector. Figure 6 shows the data plotted as fluorescence intensity at 340 nm versus intensity of the 312 nm laser pulse. A least-squares fit of the data shows a nearly cubic power dependence, indicating that the pump excitation is a three-photon process.

Figure 7 shows time-resolved data obtained from the dissociation of CH_2I_2 , CH_2Br_2 and CH_2Cl_2 . Each transient was obtained by multiphoton excitation at 312 nm, followed by depletion probing at 624 nm from the D' state of the relevant diatomic halogen product. The polarization vectors of pump and probe pulses were aligned parallel to each other. Fluorescence was detected at the wavelength corresponding to the maximum intensity of the appropriate $D' \rightarrow A'$ transition. Figure 7 shows that in each case, the fluorescence is depleted at positive times (probe pulse following pump, to the right of time zero). The intense features at time zero (pump and probe pulses overlapped in time) are due to a cooperative multiphoton effect which enhances the fluorescence signal. In this region, the molecules absorb 312 and 624 nm photons simultaneously. This leads to an enhancement in the fluorescence signal if it opens up another reaction pathway for the production of $X_2(D')$.

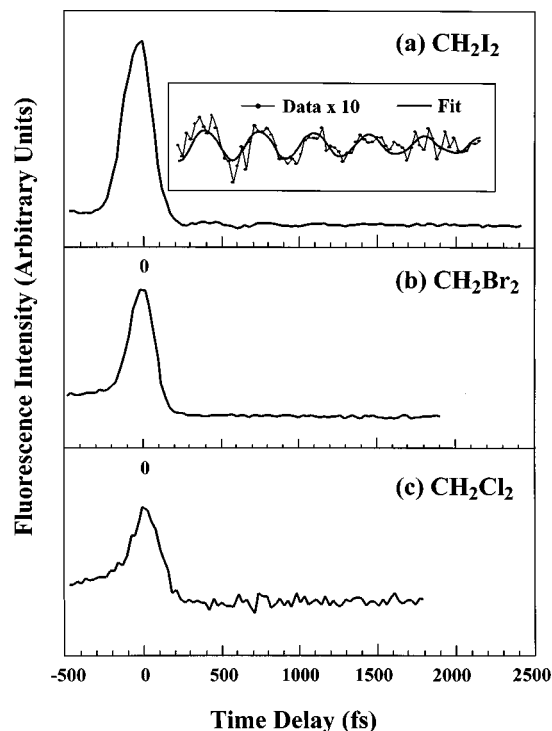


FIG. 7. Time-resolved data from the multiphoton dissociation of alkyl halides at 312 followed by probing at 624 nm and detection of the $D' \rightarrow A'$ transition. (a) From the dissociation of CH_2I_2 , by detection of $I_2(D')$ at 340 nm. The inset shows the positive time data multiplied by a factor of ten, along with a least-squares fit obtained using a bimodal Gaussian distribution of vibrational levels (see text). The observed fit was obtained using two modes, the first centered at $v' = 19$ and having a FWHM of 7. The second contribution is from a mode with an oscillation frequency of 104 cm^{-1} , having a FWHM approximately equivalent to one vibrational level in the D' state. (b) Time-resolved data of the molecular detachment of Br_2 from CH_2Br_2 show depletion at positive times, and a strong time zero feature. The transient was obtained by detecting the $Br_2 D' \rightarrow A'$ fluorescence at 287 nm. (c) The transient of CH_2Cl_2 was obtained by detection at 254 nm. This reaction yielded much lower signals, therefore the noise level is higher, but depletion by the 624 nm pulse at positive times is clear.

Figure 7 also clearly shows vibrational coherence in the I_2 fragment after photodissociation of CH_2I_2 . This is an indication that the process responsible for formation of the halogen molecules is concerted, since in-phase vibrations could not result unless the molecules are formed within a short time of each other and on the same region of the product potential energy surface (PES). The fundamental frequency of Br_2 in the D' state is 150.86 cm^{-1} ,³² which corresponds to a vibrational period of 221 fs. While vibrational coherence in the Br_2 fragment has not to date been resolved, further efforts to do so are underway. The fundamental frequency of Cl_2 in the D' state is 252.43 cm^{-1} ,³⁴ which corresponds to a vibrational period of 132 fs. Since observation of vibrational modulation depends upon the convolution of the molecular dynamics with the pulses, a 60 fs pulsewidth does not allow us to observe vibrational coherence in the Cl_2 fragment. The low signal to noise ratio in both the spectral and dynamic data from the CH_2Cl_2 sample is due to rather weak fluorescence from the nascent Cl_2 fragment.

Figure 8 shows transients obtained from the CH_2I_2 cell when pump and probe lasers were polarized parallel and perpendicular to each other. There is not sufficient anisotropy in

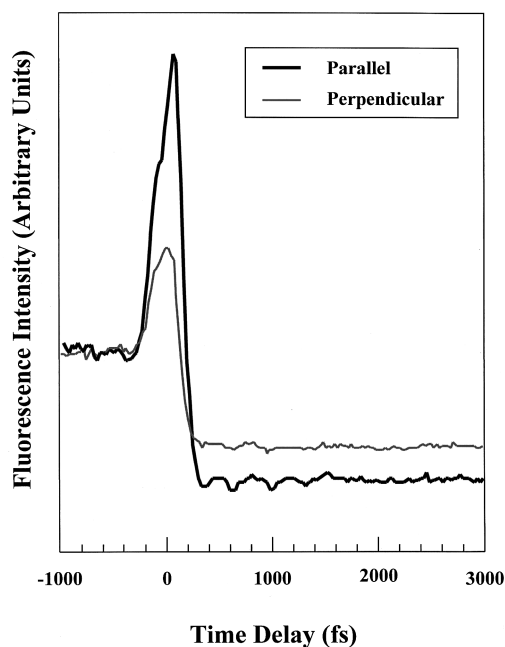


FIG. 8. Time-resolved data of the CH_2I_2 dissociation obtained with parallel and perpendicular configurations. Parallel and perpendicular refer to the polarization vectors of the pump and probe pulses relative to each other. Note the difference in intensity of the time zero feature between the parallel and perpendicular polarization configurations. The anisotropy data are ambiguous; no reliable conclusions about the rotational population of the products can be drawn from analysis of these data.

the data to obtain reliable information about the rotational dephasing time of the molecules. The fact that time zero enhancement is greater when the 624 nm pulse is polarized parallel to the 312 nm pulse further confirms that this feature is due to a cooperative process.

IV. DISCUSSION

A. Spectroscopy

The excited state of CH_2I_2 which is being accessed by the excitation is unknown. The first excited state has an absorption near $32\,000\text{ cm}^{-1}$, which corresponds to a single photon at 312 nm. This state has B_1 symmetry,^{10–12} for a three-photon process, resonant enhancement via this state would also reach a B_1 dissociative state. However, a state of this symmetry has a node between the iodine atoms, which precludes the formation of an interhalogen bond. Two-photon resonant enhancement at 312 nm allows access to the B_2 and A_1 excited states; there are no symmetry restrictions on forming a bond between the iodine atoms via transitions having either symmetry.

In an effort to elucidate the nature of the parent electronic state that correlates to dihalogen products, Okabe *et al.* compared the absorption spectrum of CH_2I_2 in the vacuum ultraviolet region with the fluorescence excitation spectrum in the same region (342 nm detection).⁷ The absorption and fluorescence excitation spectra both showed broad continua, which were ascribed to $\text{C-I } \sigma \rightarrow \sigma^*$ transitions. Although features assignable to Rydberg transitions appeared in the absorption spectrum, their absence from the fluorescence excitation spectrum seems to exclude the in-

volvement of Rydberg state excitation in the I_2 photodetachment process. Since molecular Rydberg states have very long lifetimes, particularly at high excitation energies (from ≈ 100 fs for low N to $\sim \mu\text{s}$ for high N), the time-resolved data presented in this work also indicate that Rydberg states are not involved in the molecular detachment process.

In our experiments we observed no evidence of molecular iodine products in any of the lower valence states. However, I_2 has a dissociation energy of 1.54 in its ground state, 0.54 in its B state and ≈ 0.3 eV in its A and A' states,³⁹ so molecular product in any of these states would dissociate rapidly under the experimental conditions because the available energy is very high. An ion-pair state, which correlates to $\text{X}^+ + \text{X}^-$, would be a good candidate for a dissociation product because these states are strongly bound and have long range attractive forces. For halogens there are 18 of these, corresponding to the 3P , 1D and 1S terms of the X^+ ion.

First tier ion-pair states have equilibrium energies within 0.16 eV of each other.⁴⁰ The two other ion-pair families are found approximately 0.9 and 1.5 eV higher.³⁹ Three-photon excitation at 312 nm is equivalent to 12 eV, which translates into an excess energy of ≈ 3 eV above the observed barrier to molecular photodetachment at 9.4 eV. This brings all the ion-pair states within energetic reach. The observed data for CH_2I_2 photodissociation indicate that only a small percentage (10%, not corrected for fluorescence yield or detection efficiency) of fluorescence occurs at wavelengths between 250 and 290 nm. These wavelengths correspond to the second tier of ion-pair states, which correlate with $\text{X}^+(^3P_0) + \text{X}(^1S)$.³⁶ The observed predominance of the D' state strongly suggests that electronic excitation directly correlates to this state. However, it is also possible that high-energy excitation of the parent molecule yields a halogen molecule in another ion-pair state while it is still close to the carbene fragment, and that under these circumstances relaxation to the D' state occurs. For example, the dissociation process itself may act as a half-collision. It is known that single collisions of most I_2 ion-pair states with buffer gases are highly efficient in causing nonradiative transitions to the D' state;³³ it is possible that the half-collision represented by the dissociation may be efficient enough to produce a similar effect.

The fits to the I_2 spectrum shown in Fig. 3(a) indicate that the population of the D' state is non-Boltzmann, i.e., nonstatistical. This would be expected in a molecule which had been excited using a femtosecond pulse, which produces a wave packet on the excited potential energy surface. The fact that the coherence in the parent molecule is preserved in the dissociation fragment, however, indicates that the reaction is completed very rapidly, before thermalization can occur. This is consistent with the observed reaction time and the vibrational coherence in the product channel.

B. Transition state dynamics

Figures 7 and 8 both show that there is a large enhancement at time zero in the 340 nm fluorescence signal from the photoinduced detachment of halogen molecules from gem-

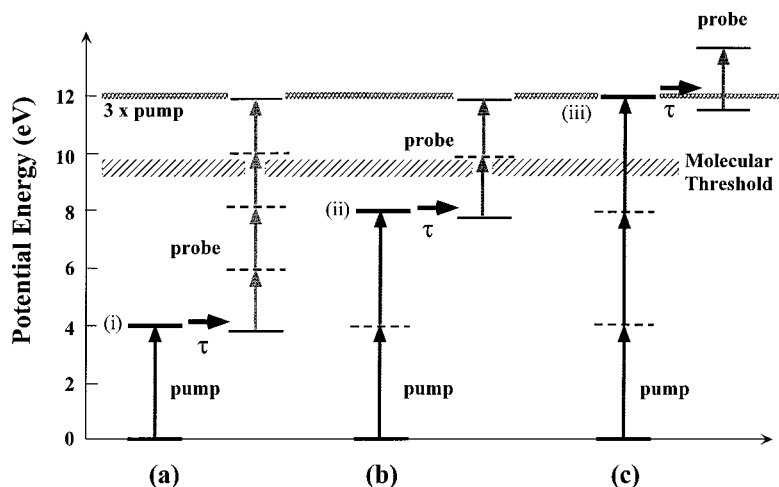


FIG. 9. Possible excitation schemes to produce time zero fluorescence enhancement. The threshold indicated is the observed excitation threshold for production of CH_2 and $\text{I}_2(D')$. The upper line on the figure corresponds to 12 eV, the excitation energy corresponding to a three-photon pump transition. (a) One-photon excitation with the 312 nm (pump) pulse requires three photons of 624 nm (probe) light to reach the threshold for production of $\text{I}_2(D')$. An additional photon of the probe produces an excitation of 12 eV. Single-photon absorption at 312 nm is equivalent to an excitation of 4 eV, which is sufficient to reach the $\tilde{A}(^1B_1)$ state of CH_2I_2 [marked (i) in the figure]. (b) An initial absorption of two pump photons corresponds to an excitation of 8 eV, requiring one photon of 624 nm light to reach the threshold and two to be equivalent to an excitation of 12 eV. The pump-excited state, marked (ii), is unknown. (c) A three-photon pump corresponds to an initial excitation of 12 eV. This is the pathway of the most interest to us because the dynamics observed between the pump and probe pulses corresponds to the transition state of the photoinduced molecular detachment reaction. The state (iii) is the dissociative state under investigation.

dihaloalkanes. This is of interest both because it can be used to yield information about the electronic structure of the parent molecule and because it affords a measure of the lifetime of the transition state for the reaction. Analysis of this can help to elucidate the nature of the reaction mechanism. We need to consider possible causes of the observed enhancement.

Figure 9 shows a schematic of the possible excitation schemes that can lead to enhancement of the fluorescence signal at time zero. The decay time of the time zero fluorescent enhancement is directly related to the lifetime of the initial excited state of the parent molecule accessed by the pump transition (which we will call the pump-excited state). The molecular dynamics is manifested as an asymmetry in the time zero peak; the decay time (on the positive side of time zero) is slower than the rise time. This allows us to determine an upper limit for the lifetime of the pump-excited state. It should be noted that the pump-probe data at time zero measure the statistical lifetime of the pump-excited state, not the time taken to reach a particular region of the potential energy surface. These data thus contain no direct information about the exit channel dynamics, but can be used to measure an upper limit for the dissociation time of the molecules.

The transition state of the photoinduced molecular detachment reaction under investigation is the state of the parent molecule accessed by a three-photon pump transition; an excitation scheme for this process is shown in Fig. 9(c). However, other excitation processes are also possible at time zero. In order to have the observed effect, the process responsible for the fluorescence enhancement must be of the general type shown, i.e., one or more 312 nm (pump) photons causes a transition to an excited electronic state. Subsequent absorption of 624 nm (probe) photons produces CH_2X_2 in a sufficiently high energy state to produce $\text{CH}_2 + \text{X}_2(D')$. There are a number of possibilities for this excitation scheme; the most plausible are shown in Fig. 9 for the example of CH_2I_2 . If the initial excitation is provided by ab-

sorption of one 312 nm photon, it requires three photons of 624 nm light to reach 10 eV, above the observed threshold for production of I_2 in the D' state,⁷ four (plus the initial one photon at 312 nm) provides the same energy as three photons of 312 nm light. This is shown as scheme (a). In either case, the state being probed is 4 eV above the ground state; observed molecular dynamics would give the statistical lifetime of this state. On the other hand, Fig. 9(b) shows the situation if the pump-excited state is reached by two pump photons. There are again two possibilities; a one-photon probe transition will exceed the threshold for production of $\text{I}_2(D')$; a two-photon probe transition accesses the same state that is reached by three photons at 312 nm. If this were the excitation scheme, the lifetime of the state 8 eV above the ground state would be reflected in the molecular dynamics. The third scheme is shown in Fig. 9(c). In this case, three photons of ultraviolet (UV) are absorbed, thus reaching the state of CH_2I_2 that we wish to examine. The lifetime of this state is probed by excitation by the 624 nm pulse to a higher energy state.

We have observed a significant enhancement to the fluorescence at time zero even for quite low intensities of 624 nm pulses. This implies that the scheme shown in Fig. 9(a) is probably not a likely alternative, since it requires at least three 2 eV photons to be absorbed as the probe. Scheme (c) would allow the lifetime of the transition state to be determined; scheme (b) would yield molecular dynamic information characteristic of the lifetime of another electronic state than the one of interest. We cannot determine at this time which is more likely. However, it should be noted that because we are measuring an upper limit for the dissociation time, the process that produces the depletion signal cannot be slower than the dissociation time measured using the transition state dynamics.

In order to analyze the transition state dynamics of the reaction, a kinetic model was constructed for the behavior of the fluorescence signal as a function of delay time between the pump and probe pulses. Figure 10 illustrates the model.

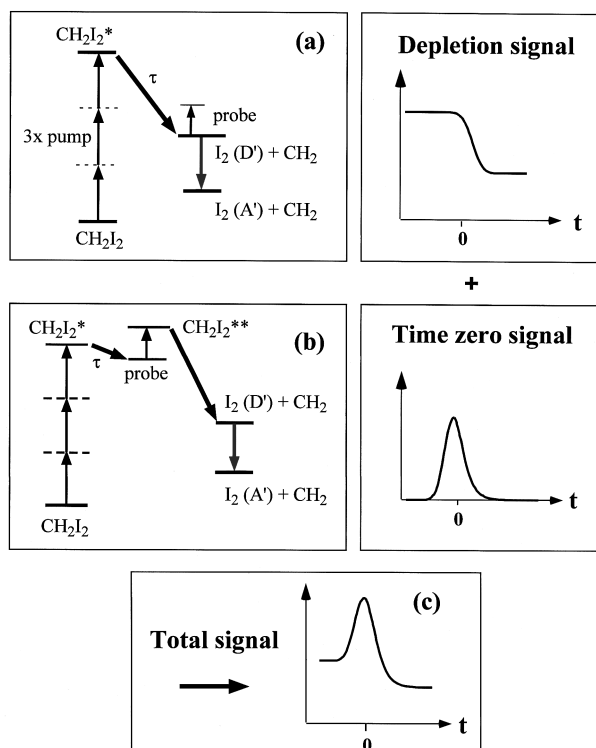


FIG. 10. Kinetic model for the dissociation of CH_2I_2 . The model assumes that the signal is comprised of two contributions: (a) Depletion signal. This is produced by the molecular detachment process. Excitation of CH_2I_2 with three photons of 312 nm light produces an excited molecule, which dissociates into CH_2 and $\text{I}_2(D')$. Depletion of the D' fluorescence with a 624 nm pulse probes the dynamics of formation of $\text{I}_2(D')$. (b) Time zero signal. When the pump and probe pulses coincide, it is possible for CH_2I_2 to absorb probe photons prior to dissociation, which produces a highly excited parent molecule. This increases the amount of $D' \rightarrow A'$ fluorescence observed because it opens another pathway for production of $\text{I}_2(D')$. In this case, the statistical lifetime τ of the pump-excited state determines for how long after the initial excitation the molecule can absorb the probe. The overall signal is a weighted sum of these two contributions, each of which is convoluted with a Gaussian to simulate the pulsewidth.

The observed transient can be modeled as the sum of two contributions. The molecular detachment signal (a) will exhibit a step at time zero due to depletion by the 624 nm pulse. The time zero fluorescent enhancement (b) can be represented as a Gaussian-type peak decaying exponentially at positive time.

Figure 10(a) illustrates the depletion signal. Three photons of 312 nm light are absorbed by CH_2I_2 ; the molecule dissociates to produce I_2 in the D' electronic state. Detection of fluorescence from the $D' \rightarrow A'$ transition at 340 nm allows reaction dynamics to be probed by monitoring the amount of D' state population depleted by absorption of a second femtosecond pulse at 624 nm. When the probe pulse arrives before the 312 nm pulse (negative time), it does not affect the intensity of the fluorescence. Since it is the nascent product that is being probed, depletion starts to become possible once the pulses are overlapped in time; at this point, the signal level begins to drop. The amount of depletion possible increases steadily as the molecules dissociate; this continues until no more $\text{I}_2(D')$ can be formed. The molecular signal response as a function of pump-probe time delay would then be a step function with an exponential decay. To account for

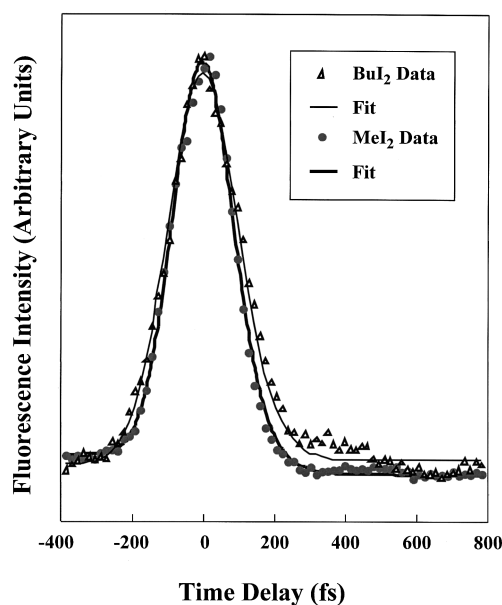


FIG. 11. Time-resolved data of the molecular photodetachment of I_2 from CH_2I_2 and $n\text{-C}_4\text{H}_8\text{I}_2$. The data are plotted as points; the fit is shown as a line in each case. The difference in dissociation time between the two molecules can be accounted for completely by the difference in mass of the alkyl fragment. The relatively poor fit to the $\text{C}_4\text{H}_8\text{I}_2$ dynamics at positive times is due to the presence of a vibrational oscillation at early times.

the temporal width of the pulses, this function is convoluted with a Gaussian; the resulting curve is shown in Fig. 10(a).

To model the intense time zero feature, a similar approach was used. In this case, there is no signal at negative times. At time zero a cooperative (multiphoton) effect occurs and signal levels reach their maximum value. As the time delay between pump and probe pulses increases, the molecules begin to dissociate and the multiphoton signal enhancement is no longer possible. Thus the time zero feature can be represented as a half exponential function as shown in Fig. 10(b). Again, this is convoluted with a Gaussian to account for the temporal pulsewidth. The overall signal should then behave as a sum of contributions from the depletion and time zero features as shown in Fig. 10(c). For simplicity, variations in the signal caused by rotational and vibrational motion of the nascent products were not included. The model does not take into account the possibility of contributions from other states, but should provide a reliable upper limit on the dissociation time for a given pulsewidth. The details of the mathematical formulation used are included in the Appendix.

Transients obtained near time zero from methylene diiodide and butylene diiodide are shown in Fig. 11. Both were taken with the polarization vectors of pump and probe lasers aligned parallel to each other. The data were fit using a nonlinear least-squares procedure and the model described above. The dissociation time of $\text{C}_3\text{H}_7\text{CHI}_2$ was found to be $\tau \leq 87 \pm 5$ fs, indicating that molecular detachment is prompt. Fitting of the CH_2I_2 time zero transient using the same method produced a dissociation time τ of 47 ± 3 fs. If we assume that the difference in dissociation time of the two molecules is caused only by the difference in reduced mass

TABLE I. Vibrational frequencies of CH₂I₂ normal modes in the ground state. Presented are the calculated (gas phase) and experimentally measured solution and liquid phase values. The vibrational frequencies were obtained at the Hartree–Fock (HF) level by optimizing the geometry of the molecule and then conducting a frequency analysis using GAUSSIAN 94 (Ref. 42). The LANL2DZ effective core potential basis set was used for the iodine atoms and the 6-31G* basis set for the hydrogen and carbon atoms. The calculated frequencies of the normal modes were scaled by 0.8929 and the zero-point energy by 0.9135 (Refs. 43 and 44).^a

Peak	Type	Calculated Gas phase ^b	Experimental		
			Liquid CH ₂ I ₂ (Raman) ^c	Liquid CH ₂ I ₂ (Infrared) ^c	Cyclohexane solution (Raman) ^d
ν_4	I-C-I bend	117	121		134
ν_3	I-C-I symmetric stretch	454	486	486	493
ν_9	I-C-I asymmetric stretch	552	567	573	581
ν_7	CH ₂ rock	716	714	717	714
ν_5	Torsion	1056	1028		1028
ν_8	CI ₂ rock	1148	1104	1106	
ν_2	H-C-H bend	1374	1350	1351	1369
ν_1	H-C-H symmetric stretch	2958	2968	2967	2968
ν_6	H-C-H asymmetric stretch	3043	3049	3049	3049

^aAll values given in cm⁻¹.

^bThis work; calculated using GAUSSIAN 94 as stated in text.

^cSee Reference 45.

^dReference 18.

μ , we can use the following relationship to predict the expected difference in dissociation time:

$$\left(\frac{\tau_{\text{MeI}_2}}{\tau_{\text{BuI}_2}}\right) = \sqrt{\frac{\mu_{\text{BuI}_2}}{\mu_{\text{MeI}_2}}}. \quad (1)$$

This expression applies if the fragments have the same amount of kinetic energy in both cases, the right-hand side yields a ratio of 0.538. The observed ratio obtained from the fit $\tau_{\text{MeI}_2}/\tau_{\text{BuI}_2} = 0.54$. Thus the near factor of two difference in dissociation time can be completely accounted for by the mass difference, i.e., there appears to be no IVR occurring during dissociation even for a system like gem–diiodobutane in which there is a moderately large density of states.

To estimate the amount of available energy that is partitioned into center-of-mass translational motion of the fragments, we use τ as an upper limit for the dissociation time of each molecule. For the purposes of the model, we will assume τ to be the time taken for the fragments to move a distance L apart, at which point dissociation will be considered to be complete. The amplitude of the C–I stretch is ≈ 1 Å (see Table I), so it is reasonable to assume that the carbon–iodine bonds can be considered broken once the fragments have moved more than 2 Å farther apart than the equilibrium distance. A simple impulsive model can then be employed to determine the translational energy E of the fragments by assuming that they reach terminal velocity instantaneously,

$$E = \frac{1}{2}\mu\left(\frac{L}{\tau}\right)^2, \quad (2)$$

where μ is the reduced mass of the carbene and I₂ moieties, assuming they form a pseudodiatom (essentially the mass of the alkyl fragment). Using a length parameter of $L = 2.0$ Å and a dissociation time τ of 47 fs, the kinetic energy of CH₂I₂ upon dissociation is estimated to be 1.26 eV.

C. Vibrational analysis

The transient shown in Fig. 7 was produced from the dissociation of CH₂I₂ when pump and probe lasers were polarized parallel to each other. The modulation in signal intensity at positive times is indicative of vibrational coherence in the I₂ product, which requires that the molecular detachment process be concerted. It was not possible to perform Fourier transform analysis of the data because the vibrational modulation dephases quickly and does not seem to recur (see Fig. 8). An alternative method had to be found, therefore. The simplest method for analysis of a rapidly dephasing oscillatory signal of this type is a damped sinusoidal function of the form,

$$A + Be^{-t/\tau} \cos(\omega t + \phi), \quad (3)$$

where A and B are experimentally determined parameters, τ is the dephasing time, ω the vibrational frequency and ϕ the phase. The data shown in Fig. 7 were fit using this model and were found to have an oscillation frequency of 92.2 cm⁻¹, corresponding to a vibrational period of 362 fs. The dephasing time was ~ 1 ps.

Time-resolved dynamics collected at 285 and 272 nm have also been shown to exhibit vibrational coherence⁹; if this is indeed due to population in the f state (*vide supra*), the $f(^3\Pi_{0g}^+) \rightarrow B(^3\Pi_{0u})$ fluorescence would be expected to contribute to the coherences observed in the 340 nm region. The observed dephasing would then be due in part to this additional contribution to the time-resolved signal. To test this supposition, the vibrational dynamics shown in Fig. 7(a) were fit using a bimodal-type model. The displayed fit was obtained by assuming a bimodal Gaussian distribution of vibrational levels. One mode is centered at $v' = 19$ in the D' state with a full width at half maximum (FWHM) of 7. This corresponds to a vibrational spacing of 96.6 cm⁻¹, which reflects an oscillation period of 345 fs and is close to the

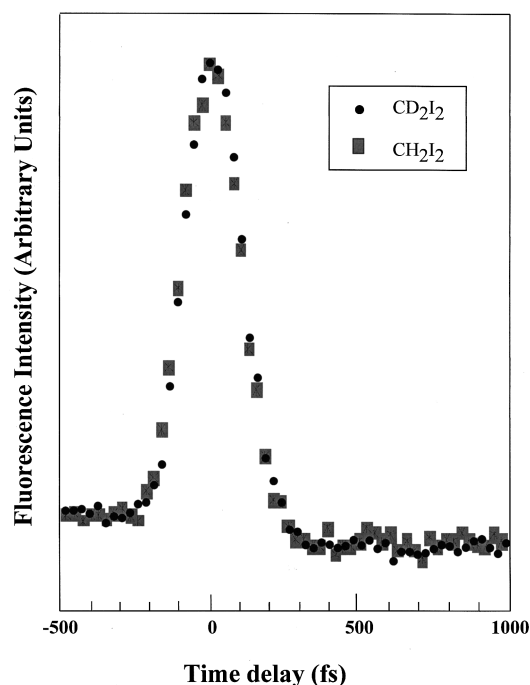


FIG. 12. Time-resolved data obtained near time zero for the high-energy dissociation of CH_2I_2 and CD_2I_2 . The dissociation time is identical for the two compounds, indicating that vibrational modes in the alkyl fragment are not involved in the dissociation mechanism (see text).

result from the damped sinusoidal model discussed above. The second mode has an oscillation frequency of 104 cm^{-1} and a FWHM equivalent to a single D' vibrational level. This mode appears to be contributing approximately 15% of the time-dependent signal at 340 nm, which is consistent with the intensity of the $f \rightarrow B$ fluorescence expected in this region.

Least-squares fitting to the dispersed fluorescence spectrum in the 290–350 nm region yielded a distribution centered at $v' = 9$ of the D' state; see Figs. 3(a) and 3(b). Clearly, there is a discrepancy between this result and the value obtained from fitting the dynamic data. The reason for this is not clear but may be due in part to the presence of fluorescence at 340 nm originating from the $f \rightarrow B$ transition.

It is clear from comparison with the fit to the spectrum of I_2 in Ar (Fig. 3) that the vibrational population is not thermal; both the spectrum and the vibrational oscillations from the CH_2I_2 sample can be fit by a Gaussian distribution of populations in the vibrational levels of the D' state.

Femtosecond studies of the reaction dynamics of Rydberg states of methyl iodide showed a substantial difference in reaction time for the photodissociation of CH_3I and CD_3I .⁴¹ The explanation proposed for this observation was that vibrational modes in the alkyl fragment are involved in the predissociation process, thus making the isotope effect for the dissociation substantial. Figure 12 shows the femtosecond transients near time zero for CH_2I_2 and CD_2I_2 ; it is apparent from the data that there is no detectable difference in dissociation time between the two molecules. This is strong evidence that vibrational modes in the alkyl fragment are not involved in the dissociation mechanism.

In order to investigate the possible contribution of vari-

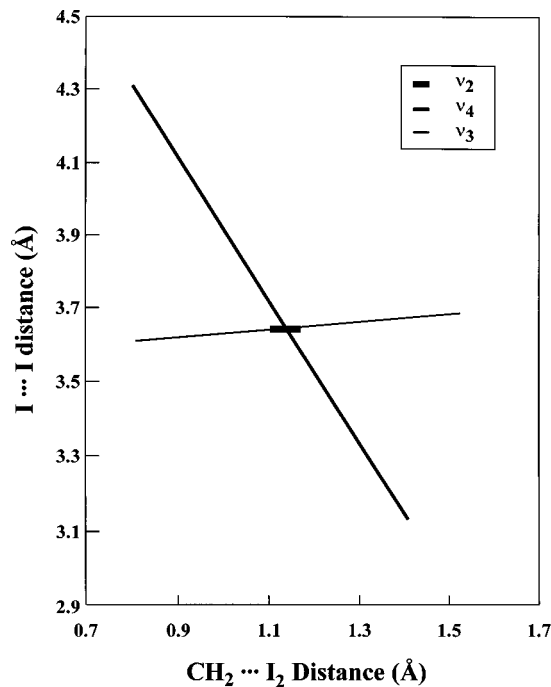


FIG. 13. Normal mode analysis of the ground state of CH_2I_2 , plotted as a function of I–I and CH_2 –I distance. Only the I–C–I bending (ν_4) and I–C–I symmetric stretch (ν_3) contribute to the I–I vibration. The other normal modes have limited or no motion between the iodine atoms.

ous vibrational modes of the parent molecule to the molecular detachment process, a frequency analysis of the ground-state equilibrium geometry of CH_2I_2 was performed using GAUSSIAN 94⁴² (for technical details see Table I caption).^{43,44}

Table I compares the normal mode frequencies of the calculated gas phase values to the experimental liquid⁴⁵ and solution phase values.¹⁸ Despite the fact that the calculated and experimental values are determined for different phases, it can be seen that the calculated frequencies are close to the experimentally observed ones (0.1%–9% deviation). The larger errors occur for those modes involving mostly iodine atom motion. This observation is not unexpected because *ab initio* calculations on molecules containing many-electron atoms like iodine are inherently less precise.

To calculate the extent of motion along the reaction coordinate for each normal mode the displacements of each atom in each normal mode were added to the equilibrium geometry configuration and single point HF calculations were conducted on these modified geometries. The energy from each single point calculation was added to the scaled zero-point energy and the resulting energy was divided by the scaled frequency for the normal mode. The result is the number of quanta in that normal mode corresponding to the atom positions calculated from the displacements. Then the normal mode displacements were scaled to find the atom positions that would correspond to one quantum of energy in each normal mode. Finally, these modified atom positions for each normal mode were mapped to the motion of the molecule along two coordinates: the distance between the two iodine atoms (I...I) and the distance between the CH_2 fragment and the I_2 fragment ($\text{H}_2\text{C}\dots\text{I}_2$) (measured from the carbon atom to the midpoint of the iodine atoms).

Figure 13 shows the results of the normal mode analysis, plotted as a function of I–I and CH₂–I₂ distance. For each mode the amplitude of the motion corresponds to one quantum of excitation in that mode. It is apparent that only the I–C–I bending ν_4 and I–C–I symmetric stretch ν_3 contribute to the I–I interatomic distance. The other normal mode has limited or no motion between the iodine atoms. The I–C–I bending contributes significantly to the H₂C...I₂ coordinate. Because ν_4 is the lowest energy mode, it is expected to be significantly populated at room temperature; at 294 K approximately 10% of the molecules have four quanta in this mode. The effects of vibrational excitation in the parent on the molecular detachment process are currently under investigation.

D. Mechanism

Photodissociation studies of alkyl iodides at 304 nm excitation energy revealed that the partitioning of available energy into IVR increased from 19% for methyl iodide to 70% in *n*-butyl iodide, an energy difference of 1 eV.^{46,47} This contrasts directly with our results, which indicate no apparent increase in IVR in the alkyl fragment on going from diiodomethane to gem-diiodobutane. A direct recoil with C_{2v} symmetry allows relatively efficient coupling between translational motion of the α -carbon and internal vibrational modes of the alkyl fragment.²² In this case, we would expect to see an increase in IVR on dissociation of gem-diiodobutane as compared to methylene iodide. Based on the dissociation time evidence, it therefore appears that the molecular detachment of halogen molecules from dihaloalkanes proceeds by a different pathway. A Hückel frontier molecular orbital study of dissociation at lower energies indicated that the “least-motion” path (in which C_{2v} symmetry is retained) is a high-energy pathway and that when the carbene moiety is allowed to slip off-center from the halogen–halogen axis, the reaction path is considerably stabilized.²² This corresponds to a pathway for the concerted elimination of the general type shown in Fig. 1(c). We tentatively advance this pathway as the mechanism for the molecular photodetachment process.

Because the carbene radical is ambiphilic, i.e., the lone pair at the front of the radical behaves as a nucleophile and the empty $p\pi$ orbital is electrophilic, an asynchronous concerted mechanism as discussed above would tend to produce charge separation in the halogen fragment.²² This is consistent with the fact that only ion-pair states of halogen molecules have been observed on the photodetachment of halogens from dihaloalkanes. In this case, an ylide-type intermediate would be stabilized by the charge distribution of the carbene fragment. Iso-diiodomethane, H₂–C–I–I has been observed in gas matrices at low energies,⁴⁸ in calculations of this system, it was found that less than 2 eV of excitation energy is required to produce this species. This is less energy than is needed to form CH₂I+I.²³ However, the bonding between the iodine atoms in this species is significantly weaker than in I₂ or I₂⁻, which may explain why CH₂+2I is the more common reaction pathway. The iodine atoms in this molecule are described as a contact ion pair in

which the charges are mostly concentrated on the iodine atoms; there is little redistribution of charge on the carbon atom.²³ This is consistent with a charge-transfer mechanism of the type proposed, even though the concerted elimination of interest in this work proceeds from a highly excited electronic state.

V. CONCLUSIONS

Photoinduced molecular detachment processes have been investigated by femtosecond pump–probe spectroscopy for methylene iodide and some related haloalkanes. It was found that multiphoton excitation of these molecules at 312 nm gives rise in every case to halogen molecules in ion-pair states, predominantly the D' state. Femtosecond time-resolved experiments performed on these dihaloalkanes show that the molecular detachment processes are extremely fast (<50 fs). Due to the large enhancement in the 340 nm fluorescence at time zero feature, it was not possible to unambiguously observe rotational anisotropy in the data.

Time-resolved data for the dissociation of methylene iodide revealed the presence of vibrational coherence in the halogen product. Analysis of the vibrational frequency of the signal confirmed the electronic state assignment of the D' state. The fit to the phase of the oscillations indicates that the two iodine atoms are at a turning point of their vibration at time zero. The observation of vibrational coherence indicates that the photodissociation is concerted, i.e., processes (b) or (c) in Fig. 1 are the most likely mechanisms for this reaction. Mechanism (a) can be ruled out as a source of the observed I₂ dynamics because if this were the pathway it would not have been possible to observe vibrational motion by the pump–probe method described.

ACKNOWLEDGMENTS

We thank Dr. P. Gross for writing the routines used for fitting spectra and for insightful discussions. We are grateful to Professor J. F. Harrison at MSU for his help with the *ab initio* calculations. The butyl diiodide used in these experiments was synthesized by Lauren Heystek. This work was partially funded by a Camille and Henry Dreyfus New Faculty Award. U.M. acknowledges funding from a James L. Dye Endowment Fellowship. E.J.B. is an NSF Doctoral Fellow. M.D. is a Beckman Young Investigator and a Packard Science and Engineering Fellow.

APPENDIX

In order to simulate the transition state dynamics of the molecular detachment reaction, the signal is treated as a sum of two contributions so that $I_{\text{total}}(t) = I_{\text{depletion}}(t) + I_{\text{timezero}}(t)$, as shown in Fig. 10.

To model the depletion dynamics, we will use a function of the form shown in Fig. 10(a). This can be represented mathematically by $\eta(t)[e^{-t/\tau} - 1]$, where $\eta(t)$ is a step function and τ represents the decay time of the transition state, which we will assume decays as an exponential. This function will be convoluted with a Gaussian to simulate the effects of the temporal width of the pulse,

$$\begin{aligned} & \frac{1}{x\sqrt{\pi}} \exp\left(-\frac{t^2}{x^2}\right) \otimes \eta(t) \left[\exp\left(-\frac{t}{\tau}\right) - 1 \right] \\ &= \frac{1}{x\sqrt{\pi}} \int_0^\infty \exp\left(-\frac{(t-\delta)^2}{x^2}\right) \exp\left(-\frac{t}{\tau}\right) dt \\ & \quad - \frac{1}{x\sqrt{\pi}} \int_0^\infty \exp\left(-\frac{(t-\delta)^2}{x^2}\right) dt, \end{aligned} \quad (\text{A1})$$

where $x = \sigma/\sqrt{4 \ln 2}$ and σ is the FWHM of the pulse. Integrating this expression over t produces the dynamic model for depletion of the molecules,

$$\begin{aligned} & \frac{1}{2x} \exp\left[\left(\frac{x}{2\tau}\right)^2 - \frac{\delta}{\tau}\right] \left[1 + \operatorname{erf}\left(\left|\frac{\delta}{x} - \frac{x}{2\tau}\right|\right) \right] \operatorname{sign}\left(\frac{\delta}{x} - \frac{x}{2\tau}\right) \\ & \quad - \frac{1}{2x} \left[1 + \operatorname{sign}\left(\frac{\delta}{x}\right) \operatorname{erf}\left(\left|\frac{\delta}{x}\right|\right) \right], \end{aligned} \quad (\text{A2})$$

where δ indicates the time delay between the pump and probe pulses.

In order to model time zero, we need the convolution of a delta function with a Gaussian. This is the second term in Eq. (A1). Thus the complete solution for the molecular dynamics of the molecules at time zero can be represented as shown,

$$\begin{aligned} & A \frac{1}{x\sqrt{\pi}} \exp\left(-\frac{t^2}{x^2}\right) \otimes \eta(t) \left[\exp\left(-\frac{t}{\tau}\right) - 1 \right] \\ & \quad + B \frac{1}{x\sqrt{\pi}} \exp\left(-\frac{t^2}{x^2}\right) \otimes \eta(t) \exp\left(-\frac{t}{\tau}\right) + C \\ &= A \exp(\alpha^2 - \beta) [1 + \operatorname{sign}(\gamma - \alpha) \operatorname{erf}(|\gamma - \alpha|)] \\ & \quad + B \operatorname{sign}(\gamma) \operatorname{erf}(|\gamma|) + C, \end{aligned} \quad (\text{A3})$$

where $\alpha = x/2\tau$, $\beta = \delta/\tau$ and $\gamma = \delta/x$.

A , B and C are experimentally determined fitting parameters, since we cannot predict *a priori* the amount that each component will contribute to the overall signal. We have made a number of assumptions and approximations in this model. First of all, in the interest of simplicity, the changes in signal caused by rotational dephasing and vibrational coherence have not been accounted for. Also, the intensity profile of the pulse in the depletion model is in fact a convolution of the three 312 nm pulses causing the initial excitation with the 624 nm (probe) pulse. For the model, the temporal width of the probe pulse as measured by frequency-resolved optical gating (FROG) was used. This introduces little error because the three-photon excitation will have a considerably narrower temporal width than the 624 nm pulse; the cross-correlation will therefore have a width very similar to that of the probe. We have also assumed that the convoluted FWHM of the pulses producing the time zero feature is the same as that used for the depletion; the assumption is necessary because the exact excitation process at time zero is not known.

- ¹H. Okabe, *Photochemistry of Small Molecules* (Wiley, New York, 1978).
- ²H. Okabe, A. H. Laufer, and J. J. Ball, *J. Chem. Phys.* **55**, 373 (1971).
- ³L. J. Butler, E. J. Hints, S. F. Shane, and Y. T. Lee, *J. Chem. Phys.* **86**, 2051 (1987).
- ⁴P. J. Dyne and D. W. G. Style, *J. Chem. Soc.* **1952**, 2122.
- ⁵D. W. G. Style and J. C. Ward, *J. Chem. Soc.* **1952**, 2125.
- ⁶C. Fotakis, M. Martin, and R. J. Donovan, *J. Chem. Soc., Faraday Trans. 2* **178**, 1363 (1982).
- ⁷H. Okabe, M. Kawasaki, and Y. Tanaka, *J. Chem. Phys.* **73**, 6162 (1980).
- ⁸G. Black, *Research on High Energy Storage for Laser Amplifiers* (Stanford Research Institute, 1976).
- ⁹Q. Zhang, U. Marvet, and M. Dantus, *J. Chem. Phys.* **109**, 4428 (1998), following paper.
- ¹⁰M. Kawasaki, S. J. Lee, and R. Bersohn, *J. Chem. Phys.* **63**, 809 (1975).
- ¹¹P. M. Kroger, P. C. Demou, and S. J. Riley, *J. Chem. Phys.* **65**, 1823 (1976).
- ¹²S. L. Baughcum and S. R. Leone, *J. Chem. Phys.* **72**, 6531 (1980).
- ¹³W. H. Pence, S. L. Baughcum, and S. R. Leone, *J. Phys. Chem.* **85**, 3844 (1981).
- ¹⁴T. F. Hunter and K. S. Kristjansson, *Chem. Phys. Lett.* **90**, 35 (1982).
- ¹⁵J. Zhang, E. J. Heller, D. Huber, D. G. Imre, and D. Tannor, *J. Chem. Phys.* **89**, 3602 (1988).
- ¹⁶J. Zhang and D. G. Imre, *J. Chem. Phys.* **89**, 309 (1988).
- ¹⁷W. M. Kwok and D. L. Phillips, *J. Chem. Phys.* **104**, 2529 (1996).
- ¹⁸W. M. Kwok and D. L. Phillips, *Chem. Phys. Lett.* **235**, 260 (1995).
- ¹⁹B. J. Schwartz, J. C. King, J. Z. Zhang, and C. B. Harris, *Chem. Phys. Lett.* **203**, 503 (1993).
- ²⁰K. Saitow, Y. Naitoh, K. Tominaga, and K. Yoshihara, *Chem. Phys. Lett.* **262**, 621 (1996).
- ²¹F. Duschek, M. Schmitt, P. Vogt, A. Materny, and W. Kiefer, *J. Raman Spectrosc.* **28**, 445 (1997).
- ²²S. R. Cain, R. Hoffmann, and E. R. Grant, *J. Phys. Chem.* **85**, 4046 (1981).
- ²³M. N. Glukhovtsev and R. D. Bach, *Chem. Phys. Lett.* **269**, 145 (1997).
- ²⁴Z. Kisiel, L. Pszczolkowski, W. Caminati, and P. G. Favero, *J. Chem. Phys.* **105**, 1778 (1996).
- ²⁵U. Marvet and M. Dantus, *Chem. Phys. Lett.* **256**, 57 (1996).
- ²⁶U. Marvet, Q. Zhang, and M. Dantus, *J. Phys. Chem. A* **102**, 4111 (1998).
- ²⁷Q. Zhang, U. Marvet, and M. Dantus, *Faraday Discuss.* **108**, 63 (1997).
- ²⁸I. Pastirk, E. J. Brown, Q. Zhang, and M. Dantus, *J. Chem. Phys.* **108**, 4375 (1998).
- ²⁹X. Zheng, S. Fei, M. C. Heaven, and J. Tellinghuisen, *J. Chem. Phys.* **96**, 4877 (1992).
- ³⁰J. Tellinghuisen, *J. Mol. Spectrosc.* **94**, 231 (1982).
- ³¹H. Hemmati and G. J. Collins, *Chem. Phys. Lett.* **75**, 488 (1980).
- ³²A. Sur and J. Tellinghuisen, *J. Mol. Spectrosc.* **88**, 323 (1981).
- ³³J. B. Koffend, A. M. Sibai, and R. Bacis, *J. Phys. (Paris)* **43**, 1639 (1982).
- ³⁴P. C. Tellinghuisen, B. Guo, D. K. Chakraborty, and J. Tellinghuisen, *J. Mol. Spectrosc.* **128**, 268 (1988).
- ³⁵P. J. Jewsbury, K. P. Lawley, T. Ridley, F. F. Al-Adel, P. R. R. Langridge-Smith, and R. J. Donovan, *Chem. Phys.* **151**, 103 (1991).
- ³⁶K. Lawley, P. Jewsbury, T. Ridley, P. Langridge-Smith, and R. J. Donovan, *Mol. Phys.* **75**, 811 (1992).
- ³⁷P. J. Wilson, T. Ridley, K. P. Lawley, and R. J. Donovan, *Chem. Phys.* **182**, 325 (1994).
- ³⁸M. Dantus, R. M. Bowman, and A. H. Zewail, *Nature (London)* **343**, 737 (1990).
- ³⁹R. S. Mulliken, *J. Chem. Phys.* **55**, 288 (1971).
- ⁴⁰K. Wieland, J. B. Tellinghuisen, and A. Nobs, *J. Mol. Spectrosc.* **41**, 69 (1972).
- ⁴¹M. H. M. Janssen, M. Dantus, H. Guo, and A. H. Zewail, *Chem. Phys. Lett.* **214**, 281 (1993).
- ⁴²GAUSSIAN 94 (Revision D.3), M. J. Frisch, G. W. Trucks, H. B. Schlegel, P. M. W. Gill, B. G. Johnson, M. A. Robb, J. R. Cheeseman, T. Keith, G. A. Petersson, J. A. Montgomery, K. Raghavachari, M. A. Al-Laham, V. G. Zakrzewski, J. V. Ortiz, J. B. Foresman, J. Cioslowski, B. B. Stefanov, A. Nanayakkara, M. Challacombe, C. Y. Peng, P. Y. Ayala, W. Chen, M. W. Wong, J. L. Andres, E. S. Replogle, R. Gomperts, R. L. Martin, D. J. Fox, J. S. Binkley, D. J. Defrees, J. Baker, J. P. Stewart, M. Head-Gordon, C. Gonzalez, and J. A. Pople (Gaussian, Inc., Pittsburgh, PA, 1995).
- ⁴³A. P. Scott and L. Radom, *J. Phys. Chem.* **100**, 16502 (1996).
- ⁴⁴J. A. Pople, A. P. Scott, M. W. Wong, and L. Radom, *Isr. J. Chem.* **33**, 345 (1993).

⁴⁵F. L. Voelz, F. F. Cleveland, and A. G. Meister, *J. Opt. Soc. Am.* **43**, 1061 (1953).

⁴⁶W. K. Kang, K. W. Jung, K.-H. Jung, and H. J. Hwang, *J. Phys. Chem.* **98**, 1525 (1994).

⁴⁷W. K. Kang, K. W. Jung, D. C. Kim, K.-H. Jung, and H.-S. Im, *Chem. Phys.* **196**, 363 (1995).

⁴⁸G. Maier and H. P. Reisenauer, *Angew. Chem. Int. Ed. Engl.* **25**, 819 (1986).